ELSEVIER

Journal of Molecular Catalysis A: Chemical 168 (2001) 173–186

JOURNAL OF MOLECULAR CATALYSIS A: CHEMICAL

www.elsevier.com/locate/molcata

Studies on the decomposition of N_2O over Nd_2CuO_4, $Nd_{1.6}Ba_{0.4}CuO_4$ and $Nd_{1.8}Ce_{0.2}CuO_4$

L.Z. Gao[1], C.T. Au*

Department of Chemistry and Center for Surface Analysis and Research, Hong Kong Baptist University, Kowloon Tong, Kowloon, Hong Kong

Received 12 May 2000; accepted 1 November 2000

Abstract

Nd_2CuO_4, $Nd_{1.6}Ba_{0.4}CuO_4$ and $Nd_{1.8}Ce_{0.2}CuO_4$ were prepared by means of the citric acid complexing method. The catalytic performances of N_2O decomposition to N_2 over this series of K_2NF_4-type cuprates have been evaluated. Techniques such as XRD, XPS, EPR, TPD, pulsing, in situ DRIFT, and FT-Raman as well as chemical analysis were employed to investigate the nature of the active sites and to identify the possible reaction intermediates. A catalytic reaction mechanism has been proposed. The N_2O decomposition activities declined in the order of $Nd_{1.8}Ce_{0.2}CuO_4 > Nd_{1.6}Ba_{0.4}CuO_4 > Nd_2CuO_4$ when the reaction temperatures were below 400°C. Above 400°C, $Nd_{1.8}Ce_{0.2}CuO_4$ was inferior to $Nd_{1.6}Ba_{0.4}CuO_4$. The results of chemical analysis and XPS studies revealed that there are (i) Cu^{2+}, Cu^{3+}, and extra oxygen in Nd_2CuO_4; (ii) Cu^{2+}, Cu^{+}, and extra oxygen in $Nd_{1.8}Ce_{0.2}CuO_4$; and (iii) Cu^{3+}, Cu^{2+}, and oxygen vacancies in $Nd_{1.6}Ba_{0.4}CuO_4$. There are Cu^{+}, Cu^{2+}, Cu^{3+} and active oxygen species such as O^- (O_2^{2-}) or O_2^- in the used catalysts. The results of EPR, in situ DRIFT and Raman studies suggested that during N_2O decomposition NO_3^-, NO_2^-, $N_2O_2^{2-}$, NO^-, and oxygen species (O^-, O_2^{2-}, and O_2^-) were generated. The productions of NO and N_2 are competitive. The reaction mechanism includes the redox actions amidst $Cu^{+} \Leftrightarrow Cu^{2+} \Leftrightarrow Cu^{3+}$ and $O^{2-} \Leftrightarrow O^-(O_2^{2-}) \Leftrightarrow O_2^- \Leftrightarrow O_2$. Oxygen vacancies are important sites for N_2O adsorption and oxygen species O^- are required for the formation of the crucial intermediate $N_2O_2^{2-}$.

Keywords: N_2O decomposition; Nd_2CuO_4; $Nd_{1.6}Ba_{0.4}CuO_4$; $Nd_{1.8}Ce_{0.2}CuO_4$; Redox action; Intermediates

1. Introduction

The reduction of NO_x (NO, N_2O, and NO_2) is essential in environment protection. Catalysts suitable for NO decomposition are usually effective for N_2O depletion. Generally speaking, copper is a common component in deNO_x catalysts. For the copper-based catalysts, the redox of copper ions and oxygen vacancies play an important role in the catalytic conversion of NO_x [1–6]. Although a large number of papers have been published on deNO_x catalysis, the exact nature of redox action is still a controversy. Couples such as Cu^0–Cu^+ [4], Cu^+–Cu^{2+} [7–9], and Cu^{2+}–Cu^{3+} [10–12] have been proposed to be involved in deNO_x processes. Copper species such as Cu^0 [13], Cu^+ [14–17], and Cu^{2+} [18–20] have been recognized as active sites. For N_2O decomposition, the periodic oxidation and reduction of active sites has been suggested to be responsible for the development of kinetic oscillations [21]. Another

* Corresponding author. Tel.: +852-2339-7067; fax: +852-2339-7348.
E-mail address: pctau@hkbu.edu.hk (C.T. Au).
[1] Present address: Chengdu Institute of Organic Chemistry, Chinese Academy of Sciences, Chengdu 610041, China.

1381-1169/01/$ – see front matter
PII: S1381-1169(00)00526-4

essential issue in deNO$_x$ catalysis is the identification of the reaction intermediates. Surface oxygen species [8] such as O^- [22–24], O_2^- [17,22–24], and O_{ads} [25–28] are often considered to be participants in the formation of "N_xO_y" intermediates. The species such as $(Cu–O–Cu)^{2+}$, known as "extra-lattice oxygen" (ELO), was supposed to exist in Cu-ZSM-5 [29]. Species such as NO_3^- [28,30], NO_2^- at oxygen vacancies [25,31–33], and $N_2O_2^{2-}$ [34] have been considered to be intermediates for deNO$_x$ reactions.

Nitrous oxide (N_2O) (derived mainly from adipic acid synthesis and coal combustion) can destroy stratospheric ozone [35–37]. N_2O is also a by-product in NO catalytic decomposition [30]. There are mainly three groups of catalysts for N_2O decomposition, viz. (i) Cu (Co, Fe)-ZSM-5 [25,38–40], (ii) perovskite-like mixed oxides such as La_2CuO_4 and $YBa_2Cu_3O_7$ [10,11], and (iii) precious metals such as supported Rh [37] and Pd [41]. The active sites and reaction intermediates for N_2O decomposition over ion-exchanged ZSM-5 catalysts have been studied extensively; the shortcoming of this kind of materials is their low hydrothermal stability [42]. Noble metals are effective deNO$_x$ catalysts but the high cost limits their applications. Mixed cuprates are stable at 1000°C [43]; the reaction mechanism of N_2O on these perovskite-like catalysts has not been well established. One can change rather conveniently the oxidation states of the transition metals and generate oxygen vacancies or oxygen species in perovskite (ABO_3)-like oxides by the substitution of A or B with elements of lower or higher valences, respectively. It has been reported that the difference in superconductivity between La_2CuO_4 and Nd_2CuO_4 can be related to the mismatch of CuO_2 in the La–O or Nd–O lattice. In La_2CuO_4, such a mismatch puts the CuO_2 planes under compression, whereas in Nd_2CuO_4, the CuO_2 planes are under tension [44]. In La_2CuO_4, there are CuO_6 octahedra but in Nd_2CuO_4 there are CuO_4 squares. The former is p-type while the latter is n-type. Attfield et al. reported that on a Cu–Ferrierite deNO$_x$ catalyst, the Cu^{2+} species in low co-ordination are highly active [45]. In the present study, we have investigated the decomposition of N_2O over Nd_2CuO_4, $Nd_{1.6}Ba_{0.4}CuO_4$, and $Nd_{1.8}Ce_{0.2}CuO_4$ using techniques such as TPD, XPS, EPR, in situ FTIR, and FT-Raman. The aim of this work is to establish a reaction mechanism based on the information related to active sites, redox action, and reaction intermediates.

2. Experimental

The fresh Nd_2CuO_4, $Nd_{1.6}Ba_{0.4}CuO_4$, and $Nd_{1.6}Ce_{0.4}CuO_4$ samples were prepared by the citric complexing method: stoichiometric amounts of high purity oxalates of neodymium, barium, cerium, and copper were dissolved in a citric acid solution (1 M) at 80°C with constant stirring until a viscous gel was formed. The gel was decomposed abruptly to very fine powder (ca. 10 nm) at around 400°C. Then the powder was heated in air at 1100°C for 10 h. Before being tested for catalytic performance, the samples were pressed, crushed, and sieved to 100–140 mesh.

The contents of copper in different oxidation states were estimated by means of iodometry according to the procedures adopted by Harris et al. [46]. The oxygen non-stoichiometry values were estimated from the amount of Cu^{2+}, Cu^+ or Cu^{3+} present, assuming that the other ions were in the most stable oxidation states, viz. La^{3+}, Ba^{2+}, Ce^{4+}, and O^{2-}.

Powder X-ray diffraction (XRD) studies were performed on a Rigaku D-max Rotaflex diffractometer with Cu Kα radiation and Ni filter. X-ray diffraction data were collected at room temperature in the range of 5 to 80°.

EPR spectra were recorded at −196°C with a JEOL spectrometer operating in the X-band and calibrated with a DPPH standard ($g = 2.004$). About 0.2 g of catalyst was placed in a self-made quartz cell in which the sample could be treated under different atmospheres at various temperatures. Before performing the EPR studies over the fresh samples, we He-purged (flow rate, 20 ml min^{-1}) the sample at 800°C for 1 h and then cooled it down to 25°C in He. Then, N_2O (5000 ppm with He being the carrier gas; flow rate, 20 ml min^{-1}) was introduced into the quartz cell at a desired temperature for 1 h, followed by He-purging at the same temperature and liquid-nitrogen quenching before EPR analysis.

Photoelectron spectra were recorded with a SKL-12 spectrometer equipped with a Mg Kα X-ray source. The residual pressure in the analysis chamber was maintained below 10^{-9} Torr during data acquisition. The C1s peak at a binding energy of 284.6 eV was taken as internal reference.

For TPD studies, the sample (0.2 g) was placed in the middle of a quartz micro-reactor with 4 mm

i.d. The outlet gases were analyzed on line by mass spectrometry (HP G1800A). The heating rate was 8°C min^{-1}. The N_2O-TPD experiment was performed according to the following procedures: the sample was first calcined in situ at 700°C for 1 h under a flow of He (20 ml min^{-1}) and then cooled to room temperature. The sample was then kept in a flow of N_2O/He (5000 ppm N_2O, 20 ml min^{-1}) for 1 h at 300°C and subsequently, cooled to room temperature. After being He-purged at room temperature for 1 h, the sample was heated to 600°C in helium (20 ml min^{-1}). The O_2-TPD experiments were performed according to the following procedures: the fresh sample was first heated in O_2 at 800°C for 1 h, and then cooled to room temperature in O_2. After being He-purged at room temperature for 1 h, the sample was then heated to 800°C in a flow of He (20 ml min^{-1}).

Pulse reaction was carried out using a pulse microreactor system. The pulse volume was 67.5 μl. During the reaction, helium was used as the carrier gas (flow rate, 20 ml min^{-1}).

In situ DRIFT spectra were collected on a Nicolet series II magna-IR 550 spectrometer. The catalyst (approximately 30 mg) was contained in a SPECTRA TECH infrared cell of low dead-volume. The cell was heated by an electrical resistance heater and the cell temperature was measured by an Omega Series programmable temperature controller. In situ absorbance reflectance spectra were obtained at 4 cm^{-1} resolution. The spectra were then referenced to a spectrum of the catalyst collected at the same temperature under a He flow. Before spectrum collection, the cell was evacuated by pumping (5 min) to remove gaseous N_2O.

Laser FT-Raman spectra were recorded using a Nicolet 560 FT Raman spectrometer with a He–Ne laser operating at a power of 1 mW. Spectra were collected at a resolution of 4 cm^{-1}. About 0.1 g of sample was placed in a self-made quartz tube and could be treated in a mixture of N_2O/He (N_2O, 5000 ppm) at various temperatures. Before spectrum collection, the sample was purged with He (flow rate, 20 ml min^{-1}) at room temperature for 30 min.

Steady-state catalytic activities were measured between 100 and 600°C at atmospheric pressure, 1 h after performance stabilization over a fixed-bed quartz micro-reactor. The sample (100 mg) was pre-treated in situ at 800°C for 1 h in a He flow before testing. The total GHSV was 60,000 h^{-1} and the feed concentration was 0.6% N_2O with helium being the balance. Gas chromatography (Shimadzu GC-8A) and mass spectrometry (HP G1800A) were used to determine the N_2O decomposition activity.

3. Results

3.1. Structure identification and composition analysis

The XRD results of Nd_2CuO_4, $Nd_{1.6}Ba_{0.4}CuO_4$ and $Nd_{1.8}Ce_{0.2}CuO_4$ demonstrated that they are tetragonal (T′) in structure [44]. For sustaining electron neutrality, besides Cu^{2+}, there should be 30% Cu^{3+} in $Nd_{1.6}Ba_{0.4}CuO_4$ and 20% Cu^{+} in $Nd_{1.8}Ce_{0.2}CuO_4$. In fact, it is almost impossible to obtain stoichiometric $Nd_{1.6}Ba_{0.4}CuO_4$ and $Nd_{1.8}Ce_{0.2}CuO_4$ samples. Chemical analyses based on iodometric titration indicated that there are 32% Cu^{3+} in $Nd_{1.6}Ba_{0.4}CuO_4$ and 10% Cu^{+} in $Nd_{1.8}Ce_{0.2}CuO_4$. Hence, the actual compositions of these two mixed oxides are estimated to be $Nd_{1.6}Ba_{0.4}CuO_{3.96}$ and $Nd_{1.8}Ce_{0.2}CuO_{4.05}$ (Table 1). In other words, the inclusion of Ba^{2+} resulted in the generation of oxygen vacancies, whereas the inclusion of Ce^{4+} resulted in the presence of extra-oxygen in the tetragonal structure. There are 0.6% of Cu^{3+} in Nd_2CuO_4 and the actual composition of the

Table 1
Composition, surface area, and structure of Nd_2CuO_4, $Nd_{1.6}Ba_{0.4}CuO_4$, and $Nd_{1.6}Ce_{0.4}CuO_4$

Sample	Composition	Surface area (m^2/g)	Structure
Nd_2CuO_4	$Nd_2Cu_{0.94}{}^{2+}Cu^{3+}0.06O_{4.03}$	2.9	T′[a]
$Nd_{1.6}Ba_{0.4}CuO_4$	$Nd_{1.6}Ba_{0.4}Cu_{0.68}{}^{2+}Cu_{0.32}{}^{3+}O_{3.96}$	3.8	T′
$Nd_{1.8}Ce_{0.2}CuO_4$	$Nd_{1.8}Ce_{0.2}Cu_{0.10}{}^{+}Cu_{0.90}{}^{2+}O_{4.05}$	3.6	T′

[a] Tetragonal structure different from that of an ideal La_2CuO_4.

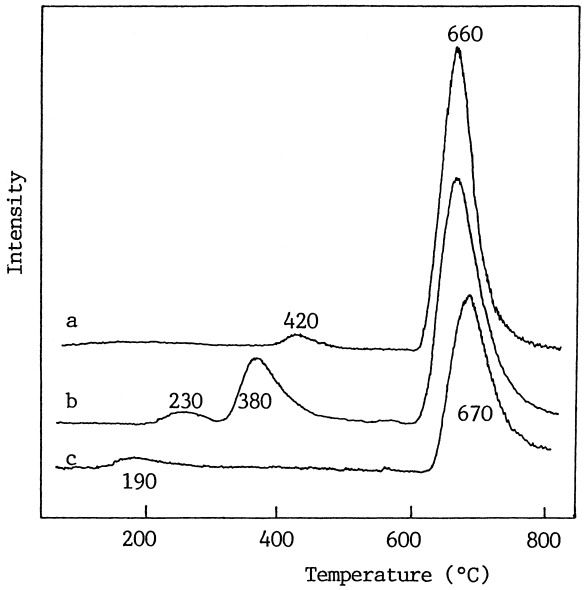

Fig. 1. O_2-TPD profiles over (a) Nd_2CuO_4, (b) $Nd_{1.8}Ce_{0.2}CuO_4$, and (c) $Nd_{1.6}Ba_{0.4}CuO_4$.

compound is $Nd_2CuO_{4.03}$, meaning that there is an excess amount of oxygen in it.

3.2. O_2-TPD studies

Fig. 1 shows the mass spectra of O_2 recorded during O_2-TPD experiments over the Nd_2CuO_4, $Nd_{1.8}Ce_{0.2}CuO_4$, and $Nd_{1.6}Ba_{0.4}CuO_4$ samples. There are O_2 desorptions at (i) ca. 420 and 660°C over Nd_2CuO_4; (ii) ca. 230, 380, and 660°C over $Nd_{1.8}Ce_{0.2}CuO_4$; and (iii) ca. 190 and 670°C over $Nd_{1.6}Ba_{0.4}CuO_4$. Generally speaking, desorptions at ca. 300–400°C are caused by the α oxygen associated with non-stoichiometric oxygen and the ones at temperatures above 650°C are caused by β oxygen related to lattice oxygen [43]. One can observe that the amount of α oxygen in the catalysts decreased in the order of $Nd_{1.8}Ce_{0.2}CuO_4 > Nd_2CuO_4 \gg Nd_{1.6}Ba_{0.4}CuO_4$.

3.3. N_2O-TPD studies

Fig. 2A–C show the mass spectra recorded during N_2O-TPD studies over Nd_2CuO_4, $Nd_{1.6}Ba_{0.4}CuO_4$ and $Nd_{1.8}Ce_{0.2}CuO_4$, respectively. For N_2 and NO, the contributions due to N_2O cracking fragments ($m/z =$ 28 and 30) have been subtracted. Over Nd_2CuO_4, N_2 desorbed at ca. 230 and 495°C; NO desorbed at ca. 120, 250, and 495°C; N_2O desorbed at ca. 110 and 495°C; O_2 desorbed at ca. 340 and above 500°C. Over $Nd_{1.6}Ba_{0.6}CuO_4$, N_2 desorbed at 170 and 360°C; NO desorbed at ca. 70, 190 and 480°C; N_2O desorbed at ca. 170 and 360°C; O_2 desorbed at ca. 350 and 500°C. Over $Nd_{1.8}Ce_{0.2}CuO_4$, N_2 desorbed at ca. 95, 205, and 500°C; NO desorbed at ca. 80, 205, and 420°C; N_2O desorbed at ca. 150, 250, and 500°C; O_2 desorbed at ca. 330 and 500°C. Over Nd_2CuO_4, N_2, NO, and N_2O desorbed largely at 495°C. Over $Nd_{1.8}Ce_{0.2}CuO_4$, large amount of N_2, NO and N_2O desorbed below 300°C. Over $Nd_{1.6}Ba_{0.4}CuO_4$, the desorptions of N_2, NO and N_2O below 400°C were considerable. The results implied that the substitution of Nd^{3+} by Ba^{2+} or Ce^{4+} had caused significant modification on the surface of the catalysts.

3.4. Pulse studies

In the effluent corresponding to a pulse of N_2O at 300°C over $Nd_{1.6}Ba_{0.4}CuO_4$, we detected NO, N_2, and NO_2; over $Nd_{1.8}Ce_{0.2}CuO_4$ or Nd_2CuO_4, we detected NO_2, NO, N_2, and O_2. If we added 5% of O_2 into the pulse of N_2O, the concentration of N_2 increased, whereas that of NO decreased over $Nd_{1.6}Ba_{0.4}CuO_4$. However, over $Nd_{1.8}Ce_{0.2}CuO_4$ or Nd_2CuO_4, similar addition of O_2 did not cause any changes in the concentrations of NO and N_2 in the effluent.

With the pre-adsorption of $^{18}O_2$ at 300°C, the pulsing of N_2O onto $Nd_{1.8}Ce_{0.2}CuO_4$ would result in the detection of $^{18}O^{16}O$ ($m/z = 34$) and $N^{18}O^{16}O$ ($m/z = 48$). The results suggest that surface oxygen species are involved in the N_2O decomposition processes.

3.5. EPR studies

Fig. 3 shows the EPR spectra of fresh Nd_2CuO_4, 600°C- and 800°C-heated (in He flow) Nd_2CuO_4, as well as N_2O-exposed (at 600°C) Nd_2CuO_4. The EPR spectrum of fresh Nd_2CuO_4 (Fig. 3a) shows the characteristic features of $Cu^{2+}(d^9)$ [34]. When the sample was heated in He at 600°C for 2 h, we observed a weak signal with $g = 2.042$ which is attributable to

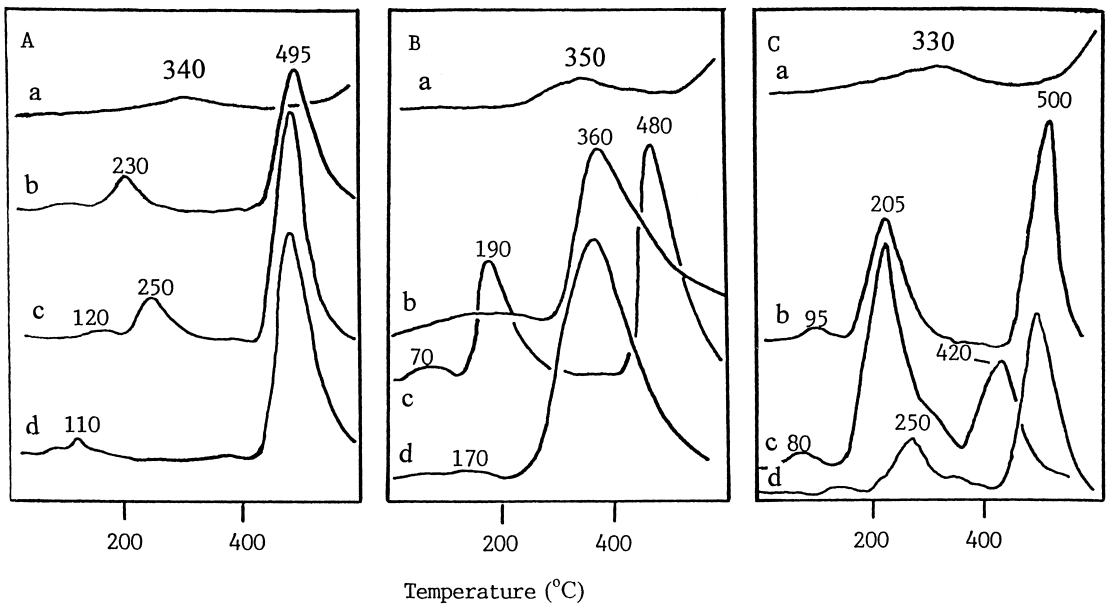

Fig. 2. Mass spectra recorded during N_2O-TPD studies over (A) Nd_2CuO_4, (B) $Nd_{1.6}Ba_{0.4}CuO_4$, and (C) $Nd_{1.8}Ce_{0.2}CuO_4$; (a) O_2, (b) N_2, (c) NO, and (d) N_2O.

O_2^- [47] (Fig. 3b). When we raised the temperature to 800°C, we detected another signal with $g = 2.007$ (Fig. 3c) which is due to the trapped electrons generated during oxygen desorption

$$O^{2-}(\text{or } O^-) \Leftrightarrow \tfrac{1}{2}O_2 + 2[e^-] \quad (1)$$

where $[e^-]$ is an electron located at an oxygen vacancy.

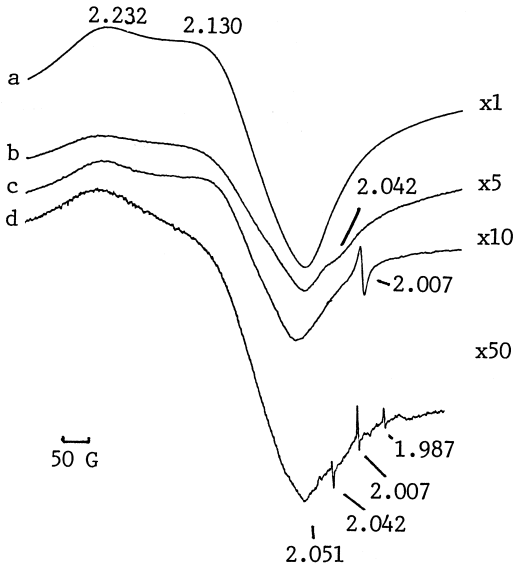

Fig. 3. EPR spectra of (a) fresh, (b) 600°C-heated, (c) 800°C-heated, and (d) N_2O-exposed (at 600°C) Nd_2CuO_4.

When we flowed N_2O into the sample cell at 600°C (Fig. 3d), we detected a signal with $g = 1.987$ which is attributable to NO–Cu^+ [34] and signals with $g = 2.009$ and 2.042 which are caused by O_2^-. Fig. 4 shows the EPR spectra of fresh, 600°C-heated (in He flow), and N_2O-exposed (at 600°C) $Nd_{1.8}Ce_{0.2}CuO_4$. In the EPR spectrum of fresh $Nd_{1.8}Ce_{0.2}CuO_4$ (Fig. 4a), we detected the signals of O_2^- ($g = 2.007$ and 2.042) and a signal at $g = 2.079$ which is a contribution of Cu^{2+} in a new co-ordination environment [34]; a signal at $g = 2.054$ which attributable to O^- was also detected [48]. When $Nd_{1.8}Ce_{0.2}CuO_4$ was heated at 600°C, the signals of O_2^- ($g = 2.007$ and 2.042) weakened (Fig. 4b). After the flowing of N_2O onto the sample (Fig. 4c), we detected NO–Cu^+ ($g = 1.989$), O_2^- ($g = 2.007$ and 2.042), O^- ($g = 2.054$), and NO radicals ($g = 1.889$) [47]. The EPR spectra of the fresh, 600°C-heated, and N_2O-exposed (at 600°C) $Nd_{1.6}Ba_{0.4}CuO_4$ samples are shown in Fig. 5. In the EPR spectrum of fresh $Nd_{1.6}Ba_{0.4}CuO_4$ (Fig. 5a),

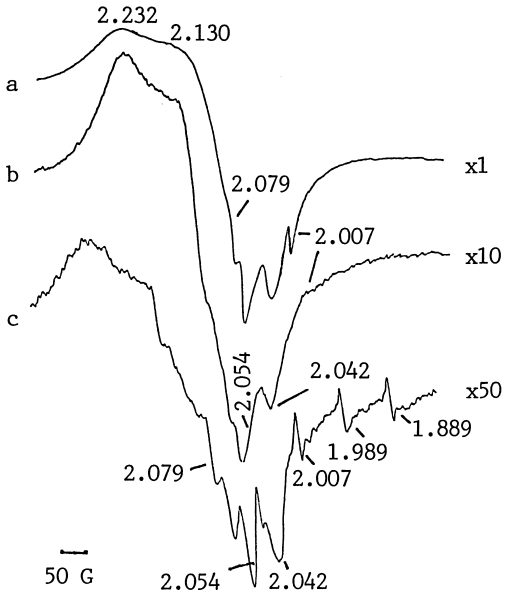

Fig. 4. EPR spectra of (a) fresh, (b) 600°C-heated, and (c) N_2O-exposed (at 600°C) $Nd_{1.8}Ce_{0.2}CuO_4$.

we detected a signal ($g = 2.079$) of Cu^{2+}. When the sample was heated at 600°C for 2 h, we detected the signals of O^- ($g = 2.054$), O_2^- ($g = 2.007$ and 2.042), and Cu^{2+} ($g = 2.079$) (Fig. 5b). After adsorption of N_2O at 600°C, we detected O_2^- ($g = 2.007$ and 2.042), O^- ($g = 2.054$), NO–Cu^+ ($g = 1.989$) and NO radicals ($g = 1.889$) (Fig. 5c). The intensity ratio of signals with $g = 2.007$ in Figs. 3d, 4b, and 5c is 5/9/14, suggesting that the concentrations of the O_2^- species generated in N_2O decomposition at 600°C over the catalyst surfaces are in the order: $Nd_{1.6}Ba_{0.4}CuO_4$ > $Nd_{1.8}$ $Ce_{0.2}CuO_4$ > Nd_2CuO_4. The intensity ratio of signals with $g = 2.054$ in Figs. 4b and 5c is 60/1, indicating that the amount of O^- species on the $Nd_{1.8}Ce_{0.2}CuO_4$ sample is larger than that on the $Nd_{1.6}Ba_{0.4}CuO_4$ sample.

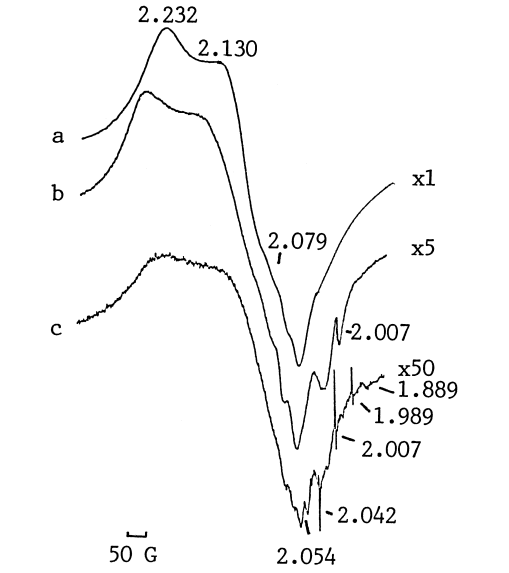

Fig. 5. EPR spectra of (a) fresh, (b) 600°C-heated, and (c) N_2O-exposed (at 600°C) $Nd_{1.6}Ba_{0.4}CuO_4$.

3.6. XPS studies

The XPS lines of the Cu $2p_{3/2}$ level of Nd_2CuO_4, $Nd_{1.6}Ba_{0.4}CuO_4$ and $Nd_{1.8}Ce_{0.2}CuO_4$ are shown in Fig. 6. For Nd_2CuO_4, the spectrum consists of a Cu $2p_{3/2}$ peak at 933.5 eV (binding energy) and a satellite

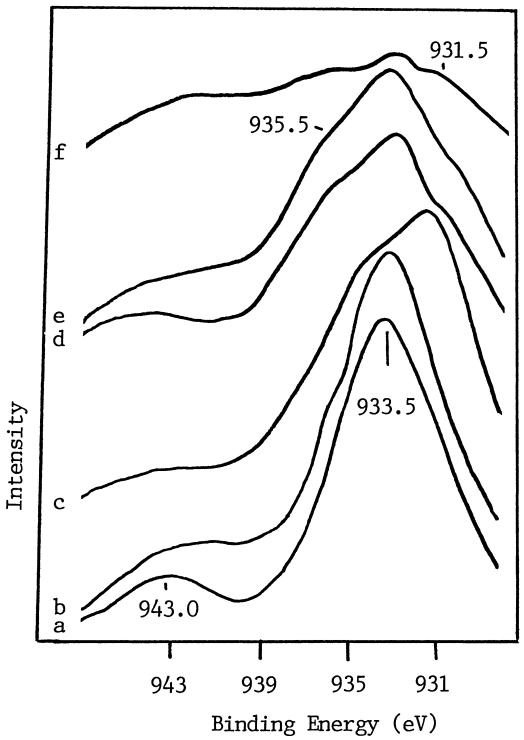

Fig. 6. Cu $2p_{3/2}$ XPS spectra of fresh (a) Nd_2CuO_4, (b) $Nd_{1.6}Ba_{0.4}CuO_4$, and (c) $Nd_{1.8}Ce_{0.2}CuO_4$; and (d) Nd_2CuO_4, (e) $Nd_{1.6}Ba_{0.4}CuO_4$, and (f) $Nd_{1.8}Ce_{0.2}CuO_4$ after being used in N_2O decomposition.

peak at 943.0 eV, indicating that in this sample, there are Cu^{2+} ions [49]. For $Nd_{1.6}Ba_{0.4}CuO_4$, there are components at 933.5 and 935.5 ev as well as a satellite peak at 943.0 eV. The peak with binding energy at 935.5 eV is attributable to Cu^{3+} as in the case of $La_{1.85}Sr_{0.15}CuO_4$ [50]. The results indicate that due to Ba^{2+} inclusion, Cu^{3+} ions were generated. In the XPS spectrum of $Nd_{1.8}Ce_{0.2}CuO_4$, there are peaks at 931.5 and 933.5 eV, as well as a satellite peak at 943.0 eV. The one at 931.5 eV can be due to Cu^{+} or Cu^{0} [49]. Considering that the presence of metallic copper is unlikely in the structure, we take that it is due to Cu^{+}. The XPS lines after N_2O adsorption on these three samples exhibit a profile with components centered at ca. 931.5, 933.5, and 935.5 eV, suggesting that after N_2O decomposition, there are Cu^{3+}, Cu^{2+}, and Cu^{+} on the surfaces of the three samples (Fig. 6d–e). The reduction in Cu $2p_{3/2}$ peak area after N_2O reaction over $Nd_{1.8}Ce_{0.2}CuO_4$ could be a result of the formation of an overlayer of nitrate/nitrite on the catalyst surface.

Fig. 7a, b, and c shows the O $1s_{1/2}$ spectra of Nd_2CuO_4, $Nd_{1.6}Ba_{0.4}CuO_4$ and $Nd_{1.8}Ce_{0.2}CuO_4$, respectively. For $Nd_{1.8}Ce_{0.2}CuO_4$ and Nd_2CuO_4, the O $1s_{1/2}$ profiles contain components at 529.5 and 531.8 eV, the former is due to lattice oxygen and the latter is due to adsorbed oxygen, probably in the forms of O_2^- and O^- (or O_2^{2-}) [51,52]. For $Nd_{1.6}Ba_{0.4}CuO_4$, there was only lattice oxygen (529.5 eV). After N_2O adsorption, there were lattice and adsorbed oxygen on the surfaces of the three catalysts (Fig. 7d–f).

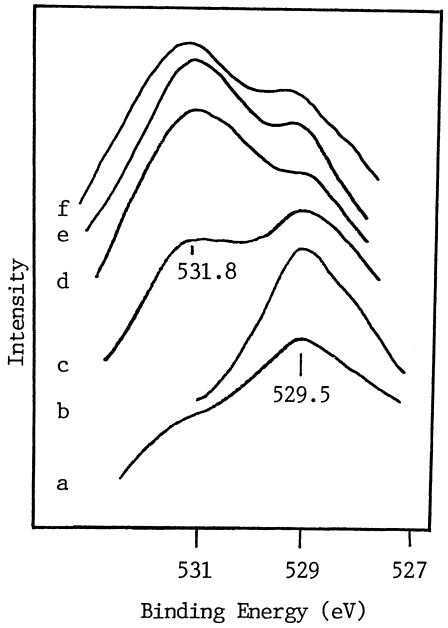

Fig. 7. O $1s_{1/2}$ XPS spectra of fresh (a) Nd_2CuO_4, (b) $Nd_{1.6}Ba_{0.4}CuO_4$, (c) $Nd_{1.8}Ce_{0.2}CuO_4$; and (d) Nd_2CuO_4, (e) $Nd_{1.6}Ba_{0.4}CuO_4$, and (f) $Nd_{1.8}Ce_{0.2}CuO_4$ after being used in N_2O decomposition.

Table 2
IR band assignments of NO_x adspecies

Wavenumber (cm^{-1})	Assignment	Reference
1879	N_2O_3	[53,54]
1747	N_2O_4	[55]
1734	$N_2O_2^{2-}$	[56]
1672	NO_2	[57]
1630	NO_2^- or $NO_2^{\delta+}$	[57–59]
1364	NO_2^- (chelating) (ν_{ONO})	[60]
1174	chelating nitrite	[47]
1060	nitrate NO_3^-	[60]

3.7. In situ FTIR studies

The FTIR assignments of N_2O-related adspecies according to the literature [47,53–60] are listed in Table 2. The in situ DRIFT spectra of N_2O adsorption on Nd_2CuO_4, $Nd_{1.6}Ba_{0.4}CuO_4$ and $Nd_{1.8}Ce_{0.2}CuO_4$ at 300°C are shown in Fig. 8a, b, and c, respectively. In the spectra, we observed (i) a strong band at ca. 1730 cm^{-1} (at ca. 1708 cm^{-1} in Fig. 8c) which

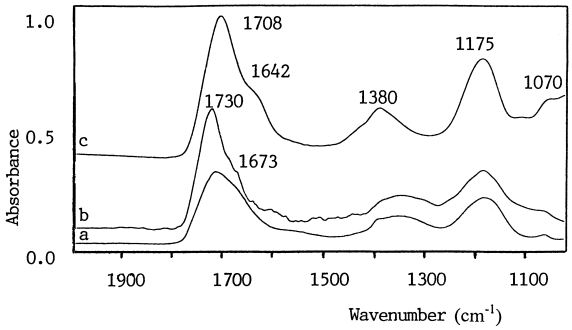

Fig. 8. In situ DRIFT spectra obtained after N_2O adsorption on (a) Nd_2CuO_4, (b) $Nd_{1.6}Ba_{0.4}CuO_4$, and (c) $Nd_{1.8}Ce_{0.2}CuO_4$ at 300°C.

Table 3
Assignment of Raman shifts

Raman shift (cm^{-1})	Assignment	Reference
1634, 1410, 732	Nitrate	[61]
1335, 820	Nitrite	[61]
1235	Nitro	[61]
1120	O_2^-	[62]
840, 960	O_2^{2-}	[63]
826, 814	O_2^{2-} in oxygen defect	[64]

can be assigned to $N_2O_2^{2-}$, (ii) a strong band at ca. 1380 cm^{-1} which can be assigned to NO_2^-, (iii) a strong band at ca. 1175 cm^{-1} which can be assigned to chelating nitrite, (iv) a weak band at ca. 1070 cm^{-1} which can be assigned to nitrate, and (v) a weak band at ca. 1673 cm^{-1} (at ca. 1642 cm^{-1} in Fig. 8c) which can be assigned to NO_3^-.

3.8. Raman studies

The assignment of Raman shifts related to nitro and nitrate as well as O_2^{2-} according to the literature [61–64] are listed in Table 3. Fig. 9a, b, and c show the Raman spectra obtained after N_2O adsorption on the Nd_2CuO_4, $Nd_{1.6}Ba_{0.4}CuO_4$ and $Nd_{1.8}Ce_{0.2}CuO_4$ samples, respectively. N_2O adsorption on Nd_2CuO_4 generated the bands of nitrate (at ca. 1650, 1430, and 720 cm^{-1}), nitro (at ca. 1280 cm^{-1}) and O_2^{2-} (at 850 cm^{-1}). N_2O adsorption on $Nd_{1.8}Ce_{0.2}CuO_4$ generated the bands of NO_3^- (at ca. 1650, 1430, and 730 cm^{-1}), nitro (at ca. 1290 cm^{-1}), and O_2^{2-} (at ca. 850 cm^{-1}). N_2O adsorption on $Nd_{1.6}Ba_{0.4}CuO_4$ generated the bands of NO_3^- (at ca. 1680, 1650, 1610, 1420, and 730 cm^{-1}), nitro (at ca. 1250 cm^{-1}), and O_2^{2-} (at ca. 910 cm^{-1}).

3.9. N_2O decomposition activities

Fig. 10 shows the N_2O decomposition activity over the Nd_2CuO_4, $Nd_{1.8}Ce_{0.2}CuO_4$, and $Nd_{1.6}Ba_{0.4}CuO_4$ catalysts. The conversion of N_2O over the catalysts declined in the order of $Nd_{1.8}Ce_{0.2}CuO_4$ > $Nd_{1.6}Ba_{0.4}CuO_4$ > Nd_2CuO_4 when the reaction temperatures were below 400°C. Above 400°C, the trend changed to $Nd_{1.6}Ba_{0.4}CuO_4$ > $Nd_{1.8}Ce_{0.2}CuO_4$ > Nd_2CuO_4. Compared to that of La_2CuO_4 [10], the decomposition activity over Nd_2CuO_4 is higher, indicating that a n-type K_2NiF_4-type cuprate is more suitable for N_2O decomposition.

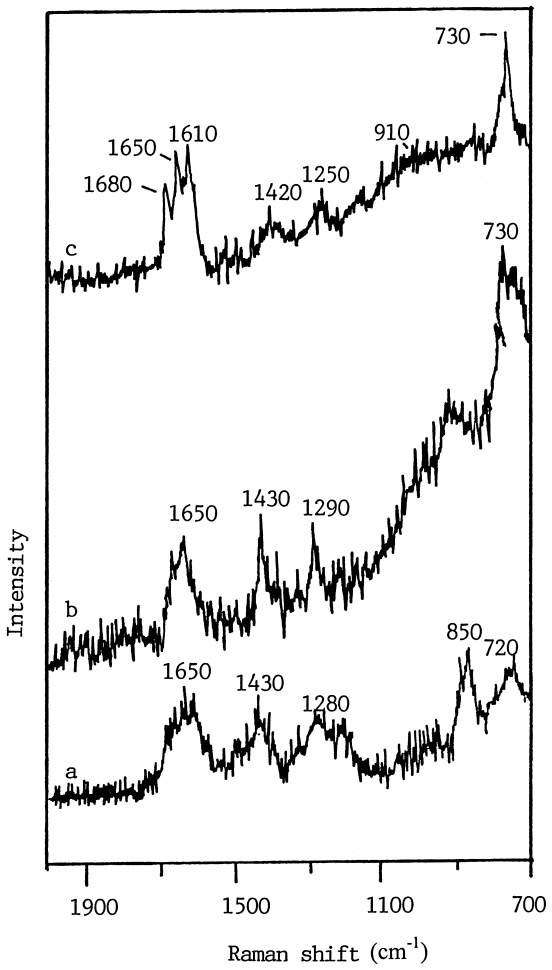

Fig. 9. FT-Raman spectra obtained after N_2O adsorption on (a) Nd_2CuO_4, (b) $Nd_{1.8}Ce_{0.2}CuO_4$ and (c) $Nd_{1.6}Ba_{0.4}CuO_4$ at 300°C.

3.10. Catalyst composition after O_2 desorption at 400 and 800°C, and after N_2O decomposition reaction

Based on the results of chemical analysis, the compositions of Nd_2CuO_4, $Nd_{1.6}Ba_{0.4}CuO_4$, and $Nd_{1.8}Ce_{0.2}CuO_4$ subjected to O_2-TPD at 400 and 800°C as well as to N_2O decomposition reaction were calculated and are listed in Table 4. One can see that after being heated at 800°C, all the three samples were reduced and oxygen vacancies were

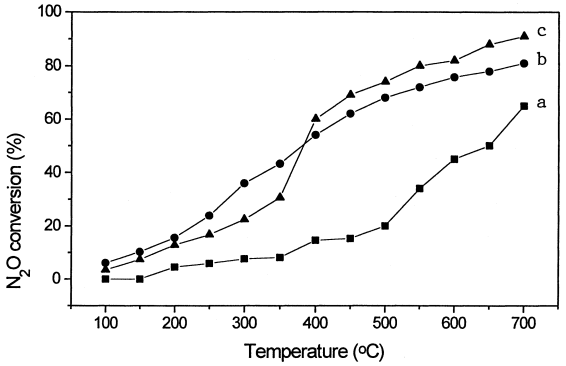

Fig. 10. Steady-state conversion–temperature plots of N_2O decomposition over (a) Nd_2CuO_4, (b) $Nd_{1.8}Ce_{0.2}CuO_4$, and (c) $Nd_{1.6}Ba_{0.4}CuO_4$.

generated. Compared to the fresh samples (Table 1), we found that the reduction and oxidation of Cu^{2+} occurred on all of the three samples during the N_2O decomposition reaction.

4. Discussion

4.1. N_2O active sites

Nd_2CuO_4 is tetragonal (T′) (Fig. 11). There is a sequence of $|CuO_2|Nd–O_2–Nd|CuO_2|$, i.e. fluorite layer and CuO_2 sheet, in this structure [44,65]. In order to retain electron neutrality, the substitution of Nd^{3+} with Ba^{2+} would result in the formation of oxygen vacancies or the oxidation of Cu^{2+}; whereas the substitution of Nd^{3+} with Ce^{4+} would lead to the presence of extra oxygen or the reduction of Cu^{2+}. The extra oxygen or oxygen vacancies can exist in the CuO_2 sheet in the form of $|CuO_{2+x}|Nd–O_2–Nd|CuO_{2+x}|$ or $|CuO_{2-x}|Nd–O_2–Nd|CuO_{2-x}|$, respectively. The interstitial oxygen or oxygen vacancies can either present in the fluorite layer as $|CuO_2|Nd–O_{2+x}–Nd|CuO_2|$ or $|CuO_2|Nd–O_{2-x}–Nd|CuO_2|$, respectively. The CuO_2 sheet is responsible for the redox action. There would be O_2^{2-} or O^- in the oxygen-excess structure. It has been reported that there are O^- species in $La_2CuO_{4+\delta}$, and the compound $La_2CuO_{4+\delta}$ can be described as: $La_2(Cu^{2+}{}_{1-x}Cu^{3+}{}_x)O_4{}^{2-}(O^-)_\delta$ [66]. Magnone et al. [67] and Grenier et al. [68] have studied the redox of

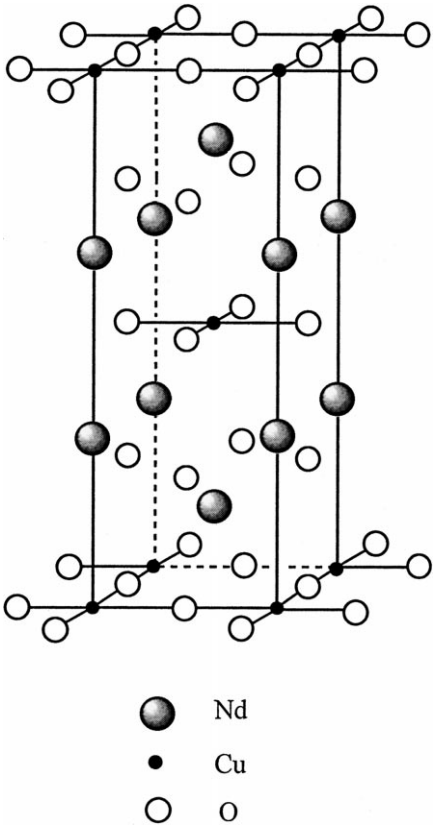

Fig. 11. Unit cell of Nd_2CuO_4.

Table 4
Compositions of Nd_2CuO_4, $Nd_{1.6}Ba_{0.4}CuO_4$, and $Nd_{1.8}Ce_{0.2}CuO_4$ after being subjected to O_2-TPD at 400 and 800°C and N_2O decomposition

	Nd_2CuO_4	$Nd_{1.6}Ba_{0.4}CuO_4$	$Nd_{1.8}Ce_{0.2}CuO_4$
400°C	$Nd_2Cu_{0.94}{}^{2+}Cu_{0.06}{}^{3+}O_{4.03}$	$Nd_{1.6}Ba_{0.4}Cu_{0.68}{}^{2+}Cu_{0.32}{}^{3+}O_{3.96}$	$Nd_{1.8}Ce_{0.2}Cu_{0.20}{}^{+}Cu_{0.80}{}^{2+}O_{4.00}$
800°C	$Nd_2Cu_{0.90}{}^{2+}Cu_{0.10}{}^{+}O_{3.95}$	$Nd_{1.6}Ba_{0.4}Cu_{0.75}{}^{2+}Cu_{0.25}{}^{3+}O_{3.93}$	$Nd_{1.8}Ce_{0.2}Cu_{0.36}{}^{+}Cu_{0.64}{}^{2+}O_{3.92}$
After reaction	$Nd_2Cu_{0.08}{}^{+}Cu_{0.85}{}^{2+}Cu_{0.07}{}^{3+}O_{4.00}$	$Nd_{1.6}Ba_{0.4}Cu_{0.04}{}^{+}Cu_{0.60}{}^{2+}Cu_{0.36}{}^{3+}O_{3.96}$	$Nd_{1.8}Ce_{0.2}Cu_{0.15}{}^{+}Cu_{0.83}{}^{2+}Cu_{0.02}{}^{3+}O_{4.03}$

O^{2-}/O^- and Cu^{3+}/Cu^{2+} in La_2CuO_4

$$Cu^{3+} + O^{2-} \Leftrightarrow Cu^{2+} + O^- \quad (2)$$

The results of chemical analysis (Table 1) and XPS studies (Fig. 6) demonstrated that besides Cu^{2+}, there are Cu^{3+} ions in $Nd_{1.6}Ba_{0.4}CuO_4$ and Nd_2CuO_4, and there are Cu^+ ions in $Nd_{1.8}Ce_{0.2}CuO_4$. EPR results demonstrated that the substitution of Nd^{3+} by Ce^{4+} or Ba^{2+} could modify the EPR feature of Nd_2CuO_4 (see Figs 3a, 4a, and 5a). O 1s spectra (Fig. 7a–c) demonstrated that there are O_2^- and O_2^{2-} (or O^-) on the fresh $Nd_{1.8}Ce_{0.2}CuO_4$ and Nd_2CuO_4 catalysts. EPR results (Fig. 3b) also suggested that there are O_2^- species on the 600°C-heated Nd_2CuO_4 sample. EPR spectra shown in Fig. 4 suggested that there are O_2^- and O^- species on the fresh and 600°C-heated $Nd_{1.8}Ce_{0.2}CuO_4$ samples.

In EPR investigations, the $Nd_{1.8}Ce_{0.2}CuO_4$ and $Nd_{1.6}Ba_{0.4}CuO_4$ oxides treated at 600–800°C showed a strong O^- ($g = 2.054$) signal, whereas Nd_2CuO_4 exhibited no significant amount of O^- signal. The $Nd_{1.8}Ce_{0.2}CuO_4$ and $Nd_{1.6}Ba_{0.4}CuO_4$ catalysts were more active than the Nd_2CuO_4 catalyst. These results suggest that surface O^- species could be related to the active sites. The intensity of the O^- signal generated in $Nd_{1.8}Ce_{0.2}CuO_4$ is 60 times of that generated in $Nd_{1.6}Ba_{0.4}CuO_4$, whereas the intensity ratio of the O_2^- signal generated in $Nd_{1.8}Ce_{0.2}CuO_4$ to that generated in $Nd_{1.6}Ba_{0.4}CuO_4$ is 9/14. Above 400°C, the N_2O decomposition activity over $Nd_{1.6}Ba_{0.4}CuO_4$ was higher than that over $Nd_{1.8}Ce_{0.2}CuO_4$. We suggest that at the temperatures above 400°C, the presence of the O_2^- species is beneficial to N_2O decomposition.

The O_2-TPD results (Fig. 1) demonstrated that there was the desorption of α oxygen from the $Nd_{1.8}Ce_{0.2}CuO_4$ and Nd_2CuO_4 samples. The desorption of lattice oxygen from the three samples was above 600°C. When Nd_2CuO_4 was treated at 600°C, O^- species were generated (Fig. 3b). Heating Nd_2CuO_4 at 800°C would lead to the generation of trapped electrons (Fig. 3c). In fresh $Nd_{1.8}Ce_{0.2}CuO_4$, there are O^- and O_2^-. Heating $Nd_{1.8}Ce_{0.2}CuO_4$ at 600°C resulted in a decrease in the intensity of the O_2^- signal (Fig. 4a and b). These results suggested that O^{2-}, O^-, O_2^- or O_2 species may transform from one another at oxygen vacancies

$$O^{2-} \Leftrightarrow O^- + e^- \quad (3)$$

$$2O^- \Leftrightarrow O_2^- + [e^-] \quad (4)$$

$$O_2^- \Leftrightarrow O_2 + [e^-] \quad (5)$$

The partial replacement of La^{3+} by Ce^{4+} in La_2CuO_4 might cause oxygen-deficiencies [69]. The EPR results demonstrated that there were O^- and O_2^- species generated in $Nd_{1.6}Ba_{0.4}CuO_4$ at 600°C (Fig. 5b). We propose that in this particular case, reactions (3) and (4) took place. In $Nd_{1.6}Ba_{0.4}CuO_4$, with the diffusion of lattice oxygen from the bulk to the surface, some of the oxygen vacancies were filled with oxygen species. In the pulse studies, the adding of 5% O_2 into the feed gas could increase the amount of N_2 production over the $Nd_{1.6}Ba_{0.4}CuO_4$ sample. The ^{18}O isotope result suggests that the surface oxygen species in the catalyst were indeed involved in the N_2O decomposition processes. We did not detect any O_2 in the outlet of a N_2O-pulse over $Nd_{1.6}Ba_{0.4}CuO_4$. We envisage that the oxygen released in N_2O decomposition remained adsorbed at oxygen vacancies in the form of O_2^- or O^-. Oxygen addition in a N_2O-pulse did not lead to an increase of N_2 over Nd_2CuO_4 and $Nd_{1.8}Ce_{0.2}CuO_4$. We detected O_2 during N_2O-pulsing over these two samples. We envisage that O_2 is relatively difficult to adsorb on an oxygen-excess cuprate. The XPS studies demonstrated that after N_2O adsorption, there were Cu^+, Cu^{2+}, and Cu^{3+} (Fig. 6) and oxygen species such as O^{2-}, O_2^-, and O^- (Fig. 7) on all of the three catalysts. The results listed in Table 4 indicated that at 400°C there were 94% Cu^{2+} and 6% Cu^{3+} in Nd_2CuO_4; 68% Cu^{2+} and 32% Cu^{3+} in $Nd_{1.6}Ba_{0.4}CuO_4$; and 20% Cu^+ and 80% Cu^{2+} in $Nd_{1.8}Ce_{0.2}CuO_4$; there were oxygen vacancies generated in $Nd_{1.6}Ba_{0.4}CuO_4$. At 800°C there were 90% Cu^{2+} and 10% Cu^+ in Nd_2CuO_4; 75% Cu^{2+} and 25% Cu^{3+} in $Nd_{1.6}Ba_{0.4}CuO_4$; and 36% Cu^+ and 64% Cu^{2+} in $Nd_{1.8}Ce_{0.2}CuO_4$; oxygen vacancies were generated in all of the three samples. These results indicated that the desorption of O_2 would cause the partial reduction of Cu^{3+} in Nd_2CuO_4 and $Nd_{1.6}Ba_{0.4}CuO_4$ and the partial reduction of Cu^{2+} in $Nd_{1.8}Ce_{0.2}CuO_4$, together with the reduction processes, oxygen vacancies were generated. The results of Table 4 and Fig. 6 indicated that in the catalysts subjected to catalytic reaction, there were Cu^+, Cu^{2+}, and Cu^{3+}, meaning that a redox action occurred during catalytic reaction. After N_2O decomposition, there were 8% Cu^+, 85% Cu^{2+} and 7% Cu^{3+} in Nd_2CuO_4; 4% Cu^+, 60% Cu^{2+}

and 36% Cu^{3+} in $Nd_{1.6}Ba_{0.4}CuO_4$; and 15% Cu^{+}, 83% Cu^{2+} and 2% Cu^{3+} in $Nd_{1.8}Ce_{0.2}CuO_4$; oxygen vacancies were generated in $Nd_{1.6}Ba_{0.4}CuO_4$. Comparing these data with the composition of the fresh samples listed in Table 1, we found that during N_2O decomposition, the reduction of Cu^{2+} to Cu^{+} and the oxidation of Cu^{2+} to Cu^{3+} occurred on all of the three samples. Based on these results, we proposed that Cu^{2+} is a major active site for N_2O decomposition. The reduction and oxidation of Cu^{2+} may result in the oscillation effect in N_2O decomposition as reported before [21]. The oxygen vacancies and oxygen species can play a role in N_2O activation. Kasai et al. reported that the oxidation of reduced copper needs oxygen [70]. Swany and co-workers suggested that N_2O adsorption occurs preferentially via the interaction of the N_2O-$\pi*$ orbitals with the cuprate oxide at the surface of $La_{1.85}Sr_{0.15}CuO_{4-y}$ [11,71]. Belapurkar et al. found that an oxygen-deficient tetragonal $YBa_2Cu_3O_6$ showed higher catalytic activity than an oxygen-rich orthorhombic $YBa_2Cu_3O_7$; they suggested that the adsorption of N_2O at oxygen vacancies would result in a change in copper valence state and the release of N_2 [72]. It was suggested that only the O_2^- species can enter the oxygen vacancies and participate in electron transfer process with the bulk [73]. With the diffusion of bulk oxygen to the surface during thermal treatment in vacuum, O_2^- species could also be formed. A O_2^- species could transform to O_2, leaving a trapped electron behind. It has been suggested by Oliver et al. that O^- and lattice oxygen O^{2-} are involved in the N_2 production steps [74].

4.2. Intermediates generated in N_2O decomposition

It has been reported that there were adspecies such as atomic oxygen and nitrate during N_2O decomposition and the adspecies changed via oscillations [21]. EPR results demonstrated that there were O^- and O_2^- species at oxygen vacancies after N_2O adsorption on the catalysts (Figs. 3–5). XPS results showed that there were lattice oxygen and adsorbed oxygen on the surface of the used catalysts (Fig. 7). Raman spectra (Fig. 9) revealed that O_2^{2-} species were generated after N_2O adsorption on the three samples. Based on these results, we concluded that the O^-, O_2^-, and O_2^{2-} species are involved in the N_2O decomposition process. It has been suggested that O^- species can be formed via the reaction [48]

$$N_2O + e^- \Leftrightarrow N_2 + O^- \quad (6)$$

Ozkan et al. deduced that the intermediate N_2O_2 could decompose to N_2O and atomic oxygen [75]

$$N_2O_2 \Leftrightarrow N_2O + O \quad (7)$$

After N_2O adsorption over the three catalysts, we detected species such as $N_2O_2^{2-}$, NO_3^-, and NO_2^- (Fig. 8). In the outlet corresponding to a N_2O-pulsing over these samples, we detected NO_2, NO and N_2. We also observed NO and N_2 desorptions during N_2O-TPD investigations (Fig. 2). In EPR studies (Figs. 3 and 5), we detected the presence of NO radicals. All the results demonstrated that NO, NO_3^-, NO_2^-, and $N_2O_2^{2-}$ are important intermediates for N_2O decomposition.

4.3. Reaction mechanism

Based on the results so far, we proposed a mechanism for N_2O decomposition

$$N_2O + [\cdot] \Leftrightarrow N_2O_{(s)} \quad (8)$$

$$N_2O_{(s)} + Cu^{n+} \Leftrightarrow N_2O^- + Cu^{(n+1)+} \quad (9)$$

$$N_2O^- + O^- (\text{or } O_2^{2-}) \Leftrightarrow N_2O_2^{2-} \quad (10)$$

$$(N_2O_2)^{2-} \Leftrightarrow 2NO^- \quad (11)$$

$$(N_2O_2)^{2-} \Leftrightarrow N_2 + O_2 + 2e^- \quad (12)$$

$$(N_2O_2)^{2-} \Leftrightarrow N_2 + O_2^{2-}(O^-) \quad (13)$$

$$O_2^{2-}(O^-) + Cu^{(n+1)+} \rightarrow O^{2-} + Cu^{(n+2)+} \quad (14)$$

$$NO^- \Leftrightarrow NO + e^- \quad (15)$$

$$O^{2-} \Leftrightarrow O^- + e^- \quad (16)$$

$$O^- + O^- \Leftrightarrow O_2^{2-} + [\cdot] \quad (17)$$

$$O_2^{2-} \Leftrightarrow O_2^- + e^- \quad (18)$$

$$O_2^- \Leftrightarrow O_2 + [e^-] \quad (19)$$

$$e^- + Cu^{(n+1)+} \Leftrightarrow Cu^{n+} \quad (20)$$

where $[\cdot]$ is the oxygen vacancy and $N_2O_{(s)}$ is the adsorbed N_2O.

According to this mechanism, $N_2O_2^{2-}$ is an essential intermediate in N_2O decomposition to NO and N_2. Surface O^- or O_2^{2-} participates in the formation of $N_2O_2^{2-}$. The productions of NO and N_2 are competitive. The EPR results indicated that the intensity trend of O_2^- signal was: $Nd_{1.6}Ba_{0.4}CuO_4$ > $Nd_{1.8}Ce_{0.2}CuO_4$ > Nd_2CuO_4. According to the results of N_2O-TPD studies, the amount of O_2 desorbed from Nd_2CuO_4 was less than those desorbed from the other two samples. This result suggested that reactions (18) and (19) are more intense over $Nd_{1.6}Ba_{0.4}CuO_4$ and $Nd_{1.8}Ce_{0.2}CuO_4$ than over Nd_2CuO_4.

For Nd_2CuO_4, there were surface oxygen species such as O_2^-. The adsorbed N_2O would interact with surface oxygen to form $N_2O_2^{2-}$. A $N_2O_2^{2-}$ intermediate decomposed to N_2 and O_2 or NO, leaving an oxygen vacancy and resulting in the reduction of Cu^{3+} and/or Cu^{2+}. On the contrary, if NO and O_2 interacted with the catalyst, Cu^{2+} could be oxidized. For $Nd_{1.8}Ce_{0.2}CuO_4$, N_2O interacted with O^- and formed $N_2O_2^{2-}$; a $N_2O_2^{2-}$ intermediate decomposed to N_2 and O_2 or NO, leaving a oxygen vacancy and resulting in the reduction of Cu^+ and/or Cu^{2+}. We suggest that the reduction of Cu^+ to Cu^0 in a K_2NiF_4-type structure is not easy, whereas the reduction of Cu^{2+} is possible. If O_2 did not desorb, Cu^{2+} and/or Cu^+ would be oxidized. At an appropriate temperature, some of the O^- in Nd_2CuO_4 and $Nd_{1.8}Ce_{0.2}CuO_4$ might dimerize to O_2^{2-}, O_2^- or O_2, and oxygen vacancies were generated. The O_2-TPD results (Fig. 1) indicated that on $Nd_{1.8}Ce_{0.2}CuO_4$, the desorption of α oxygen was significant at ca. 380°C. In this case, N_2O can readily adsorb at oxygen vacancies and react with O_2^{2-}, O_2^- or O^- to become $N_2O_2^{2-}$. In the meantime, species such as N_2O_3 and N_2O_4 may also be formed via the interaction of N_2O and surface oxygen species. However, such species were not detected in the N_2O-TPD, N_2O-pulsing, in situ DRIFT, and FT-Raman studies. It could be due to the fact that N_2O_3 and N_2O_4 are unstable and decompose readily to N_2O_2 and O. Below 400°C, N_2O adsorption on $Nd_{1.6}Ba_{0.4}CuO_4$ occurred at oxygen vacancies. In this case, a N_2O interacted with a lattice oxygen to form $N_2O_2^{2-}$. The lattice oxygen species are inactive at lower temperatures. The desorption of N_2 (without O_2 desorption) would result in the formation of oxygen species and the oxidation of Cu^{2+}. In contrast, the desorption of NO would result in the generation of more oxygen vacancies and the reduction of Cu^{2+}. Above 400°C, lattice oxygen species diffuse to the surface and interact with oxygen vacancies to become active species, possibly in the form of O_2^-. In this case, $N_2O_2^{2-}$ are formed. Thus, higher catalytic activities are achieved. The NO and oxygen species may interact with each other to form nitrate or nitrite.

Oxygen vacancies and active oxygen species are generated gradually in the three catalysts with the rise in temperature. We tentatively describe them as: $|CuO_{2+x}|Nd(Ce, Ba)–O_2–Nd|CuO_{2-y}|$ or $|CuO_{2-y}|Nd(Ce, Ba)–O_{2+x}–Nd|CuO_{2-y}|$. Consequently, high temperatures (>400°C) are favourable for N_2O conversion. Below 400°C, the catalytic activity of $Nd_{1.8}Ce_{0.2}CuO_4$ is higher than that of $Nd_{1.6}Ba_{0.4}CuO_4$. We deduce that in spite of the absence of oxygen vacancies in $Nd_{1.8}Ce_{0.2}CuO_4$, the existence of active oxygen (extra oxygen) makes the generation of $N_2O_2^{2-}$ possible. In $Nd_{1.6}Ba_{0.4}CuO_4$, there are oxygen vacancies but no active oxygen species; the adsorption of N_2O is possible but the formation of $N_2O_2^{2-}$ is difficult. As a result, the activity of $Nd_{1.6}Ba_{0.4}CuO_4$ is lower than that of $Nd_{1.8}Ce_{0.2}CuO_4$. Above 400°C, the lattice oxygen in $Nd_{1.6}Ba_{0.4}CuO_4$ gradually becomes involved and the adsorption of N_2O and the formation of $N_2O_2^{2-}$ are possible. As a result, the catalytic activity of $Nd_{1.6}Ba_{0.4}CuO_4$ increases. We thus propose that below 400°C, the formation of $N_2O_2^{2-}$ is a rate-determining step, whereas above 400°C, the adsorption of N_2O is critical. The catalytic activity of Nd_2CuO_4 are lower than that of $Nd_{1.8}Ce_{0.2}CuO_4$ or $Nd_{1.6}Ba_{0.4}CuO_4$ within the temperature range adopted for the present study; we ascribed this to the low concentrations of species O^-.

5. Conclusion

There are (i) Cu^{2+}–Cu^{3+} and extra oxygen in fresh Nd_2CuO_4; (ii) Cu^+–Cu^{2+} and extra oxygen in fresh $Nd_{1.8}Ce_{0.2}CuO_4$; and (iii) Cu^{2+}–Cu^{3+} and oxygen vacancies in fresh $Nd_{1.6}Ba_{0.4}CuO_4$. Heating the samples leads to the reduction and generation of oxygen vacancies. After N_2O adsorption, there were Cu^+, Cu^{2+}, and Cu^{3+} as well as active oxygen species on the three catalysts. We proposed that a redox action of Cu^{2+} is involved in the N_2O decomposition processes.

NO, NO_3^-, NO_2^-, $N_2O_2^{2-}$, and oxygen species are generated in N_2O decomposition. The productions of NO and N_2 are competitive. Oxygen vacancies are favourable to N_2O adsorption. Oxygen species O^- (or O_2^-) is needed for the formation of the crucial intermediate $N_2O_2^{2-}$. Below 400°C, the formation of $N_2O_2^{2-}$ is an essential step, whereas above 400°C, the adsorption of N_2O is rate-determining.

Acknowledgements

The work described above was fully supported by a grant from the Hong Kong Baptist University (FRG/97-98/I-30).

References

[1] H. Yasuda, N. Mizuno, M. Misono, Chem. Chem. Commun. (1990) 1094.
[2] C. Morterra, E. Giamello, G. Cerrato, G. Centi, S. Perathoner, J. Catal. 179 (1998) 111.
[3] J. Leglise, O. Petunchi, W.K. Hall, J. Catal. 86 (1984) 392.
[4] G. Centi, S. Perathoner, Appl. Catal. A 132 (1995) 179.
[5] N. Mizuno, Y. Fujisawa, M. Misono, J. Chem. Soc., Chem. Commun. (1989) 316.
[6] H. Shimada, S. Miyama, H. Kuroda, Chem. Lett. (1988) 1797.
[7] S.D. Peter, E. Garbowski, N. Guilhaume, V. Perrichon, M. Primet, Catal. Lett. 54 (1998) 79.
[8] A. Dandekar, M.A. Vannice, Appl. Catal. B 22 (1999) 179.
[9] M. Shelf, Chem. Rev. 95 (1995) 209.
[10] S. Subramanian, C.S. Swamy, Catal. Lett. 35 (1995) 361.
[11] J. Christopher, C.S. Swamy, J. Mol. Catal. 62 (1990) 69.
[12] H. Yasuda, T. Nitadori, N. Mizuno, M. Misono, Bull. Chem. Soc. Jpn. 66 (1993) 3492.
[13] S.C. Larsen, A. Aylor, A.T. Bell, J.A. Reimer, J. Phys. Chem. 98 (1994) 11533.
[14] D.J. Liu, H.J. Robota, Catal. Lett. 21 (1993) 291.
[15] D.J. Liu, H.J. Robota, Appl. Catal. B 4 (1994) 155.
[16] G.D. Lei, B.J. Adelman, J. Sàrkàny, W.M.H. Sachtler, Appl. Catal. B 5 (1995) 245.
[17] A.W. Aylor, S.C. Larsen, J. A Reimer, A.T. Bell, J. Catal. 157 (1995) 592.
[18] P. Bera, S.T. Aruna, K.C. Patil, M.S. Hegde, J. Catal. 186 (1999) 36.
[19] N. Mizuno, M. Yamato, M. Tanaka, M. Misono, Chem. Mater. 1 (1989) 232.
[20] A.A. Kais, A. Bennani, C.F. Aissi, G. Wrobel, M. Guelton, J. Chem. Soc., Faraday Trans. 88 (1992) 1321.
[21] S.H. Bossmann, M.F. Ottaviani, T. Turek, B. Bunsenges, J. Phys. Chem. 101 (1997) 978.
[22] G.J. Millar, A. Canning, G. Rose, B. Wood, L. Trewartha, D.R. Macinnon, J. Catal. 183 (1999) 169.
[23] A.W. Aylor, S.C. Larsen, J.A. Reimer, A.T. Bell, J. Catal. 157 (1995) 592.
[24] G. Centi, S. Perathoner, Y. Shioya, M. Anpo, Catal. Today 17 (1993) 159.
[25] P. Ciambelli, A. Di Benedetto, E. Garufi, R. Pirone, G. Russo, J. Catal. 175 (1998) 161.
[26] K.V. Ramanujachary, N. Kameswari, C.S. Swamy, J. Catal. 86 (1994) 121.
[27] L.R. Larsson, Catal. Today 4 (1989) 235.
[28] M.V. Konduru, S.S.C. Chuang, J. Phys. Chem. B 103 (1999) 5802.
[29] J. Sarkany, W.H.M. Sachtler, Catal. Lett. 16 (1992) 241.
[30] F.H.M. Dekker, S. Kraneveld, A. Briek, F. Kapteijn, J.A. Molkijn, J. Catal. 170 (1997) 168.
[31] F. Munakata, Y. Akimune, Y. Schichi, M. Akutsu, H. Yamaguchi, Y. Inoue, Chem. Commun. (1997) 63.
[32] M. Machida, H. Murakami, T. Kitsubayashi, T. Kijima, Chem. Mater. 8 (1996) 197.
[33] F. Munakata, M. Tanimura, Y. Akimune, J. Chem. Soc., Faraday Trans. 95 (1998) 933.
[34] Z. Sojka, M. Che, E. Giamello, J. Phys. Chem. B 101 (1997) 4831.
[35] M.H. Thiemens, W.C. Trogler, Science 251 (1991) 932.
[36] F. Kapteijn, J. Rodriguez-Mirasol, J.A. Moulijin, Appl. Catal. B 9 (1996) 25.
[37] K. Yuzaki, T. Yarimizu, K. Aoyagi, S. Ito, K. Kunimori, Catal. Today 45 (1998) 129.
[38] T. Turek, J. Catal. 174 (1998) 98.
[39] R.S. Cruz, A.J.S. Mascarenhas, H.M.C. Andrade, Appl. Catal. B 18 (1998) 223.
[40] M. Scher, K. Kesore, R. Monnig, W. Schwieger, A. Tissler, T. Turek, Appl. Catal. A 184 (1999) 249.
[41] O. Yuichi, K. Kazushi, B. Ming, M. Tatsuo, J. Chem. Phys. 110 (1999) 8221.
[42] J.N. Armor, Appl. Catal. B 4 (1994) N19.
[43] L.Z. Gao, Z.L. Yu, Y. Wu, Acta Chimica Sinica 55 (1997) 56.
[44] J.B. Goodenough, Supercond. Sci. Technol. 3 (1990) 26.
[45] M.P. Attfield, S.J. Weigel, A.K. Cheetham, J. Catal. 172 (1997) 274.
[46] D.C. Harris, T.A. Hewston, J. Solid. State Chem. 69 (1987) 182.
[47] A. Martinez-Arias, J. Soria, J.C. Conesa, X.L. Seoane, A. Arcoya, R. Cataluña, J. Chem. Soc., Faraday Trans. 91 (1995) 1679.
[48] T. Ito, J.X. Wang, C.H. Lin, J.H. Lunsford, J. Am. Chem. Soc. 107 (1985) 5062.
[49] P. Salvador, J.L. Fierro, J. Amador, C. Cascales, I. Rasines, J. Solid State Chem. 81 (1989) 240.
[50] M. Ospett, J. Henz, E. Kaldis, P. Wachter, Phys. C 153 (1988) 159.
[51] Y. Wu, T. Yu, B.S. Dou, C.X. Wang, X.F. Xie, Z.L. Yu, S.R. Fan, Z.R. Fan, L.C. Wang, J. Catal. 120 (1989) 88.
[52] S. Mazumdar, in: C.N.R. Rao (Ed.), Chemistry of Oxide Superconductors, Blackwell Scientific Publications, Oxford, p. 147.
[53] C.C. Chao, J.H. Lunsford, J. Am. Chem. Soc. 93 (1971) 71.
[54] I.C. Hisatsune, J.P. Devlin, Spectrochim. Acta 16 (1960) 401.

[55] G.M. Begun, W.H. Fletcher, J. Mol. Spectrosc. 4 (1960) 388.
[56] E. Giamello, D. Murphy, G. Magnacca, C. Morterra, Y. Shioya, T. Nomura, M. Anpo, J. Catal. 136 (1992) 510.
[57] A.W. Aylor, L.J. Lobree, J.A. Reimer, A.T. Bell, Stud. Surf. Sci. Catal., in: J.W. Hightower, W.N. Delgass, E. Iglesia, A.T. Bell (Eds.), Proceedings of the 11th International Congress on Catalysis, Vol. 101, 1996, p. 661.
[58] J.W. London, A.T. Bell, J. Catal. 31 (1973) 32.
[59] J.W. Neben, A.D. McElroy, H.F. Klodowski, Inorg. Chem. 4 (1965) 1796.
[60] B. Klingenberg, M.A. Vannice, Appl. Catal. B 21 (1999) 19.
[61] G. Mestl, M.P. Rosynek, J.H. Lunsford, J. Phys. Chem. B 101 (1997) 9321.
[62] R.Q. Long, H.L. Wan, Appl. Catal. A 159 (1997) 45.
[63] C.T. Au, H. He, S.Y. Lai, C.F. Ng, J. Catal. 159 (1996) 280.
[64] K. Haller, J.H. Lansford, J. Laane, J. Phys. Chem. 100 (1996) 551.
[65] J.B. Goodenough, A. Manthiram, J. Solid State Chem. 88 (1990) 115.
[66] N. Casan-Pastor, P. Gomez-Romero, A. Fuetes, J.M. Navarro, M.J. Sanchis, S. Ondono, Phys. C 216 (1993) 478.
[67] E. Magnone, G. Cerisola, M. Ferretti, A. Barbucci, J. Solid State. Chem. 144 (1999) 8.
[68] J.C. Grenier, A. Wattiaux, J.P. Doumerc, P. Dordor, L. Fournes, J.P. Chaminade, M. Pouchard, J. Solid State Chem. 96 (1992) 20.
[69] M. Daturi, G. Busca, R.J. Willey, Chem. Mater. 7 (1995) 2115.
[70] P.H. Kasai, R.J. Bishop, J. Phys. Chem. 81 (1977) 1527.
[71] K.V. Ramaujachary, C.S. Swamy, J. Catal. 93 (1985) 279.
[72] A.D. Belapurkar, N.M. Gupta, G.M. Phatak, R.M. Iyer, J. Mol. Catal. 87 (1994) 287.
[73] X. Zhang, K.J. Klabunde, Inorg. Chem. 31 (1992) 1706.
[74] C. Oliver, L. Forni, A.M. Ezerets, I.E. Mukovozov, A.V. Vishniakov, J. Chem. Soc., Faraday Trans. 94 (1998) 587.
[75] U.S. Ozkan, M.W. Kumthekar, G. Karakas, J. Catal. 171 (1997) 67.